PAPER

Check for updates

Dual inhibition of acetylcholinesterase and β-secretase by metabolites from *Echinocactus grusonii* Hildm.: *in silico* and *in vitro* investigations

Ahmed A. Heraiz, [ID] *[a] Ahmed Othman, [ID] *[a] Ahmed M. Sayed, [ID] [b]
Mostafa M. Hegazy, [ID] [a] Abd El-Salam I. Mohammed [ID] [a] and Atef A. Elhela [ID] [a]

Targeting acetylcholinesterase (AChE) and β-secretase (BACE-1) enzymes is a promising multifaceted approach for treating neurological disorders. In our study, the chemical investigation of *Echinocactus grusonii* Hildm. (Cactaceae) led to the isolation and identification of seven compounds, including three flavonoids, naringenin **1**, kaempferol **2**, and isokaempferide **3**, one megastigmane glycoside, vomifoliol-9-*O*-β-ᴅ-glucopyranoside **4**, and three alkaloids, *N*-chloromethyl hordenine **5**, *N*-acetyl hordenine **6**, and *N*-acetyl-*N*-chloromethyl-*N*-methyl tyramine **7**. Compounds **5** and **7** were identified as previously undescribed halogenated alkaloids. Biological evaluation revealed that all compounds exhibited promising acetylcholinesterase inhibitory activity (IC$_{50}$ = 0.076–2.255 μg mL^{-1}), as well as significant inhibition of β-secretase with IC$_{50}$ values ranging from 0.066 to 7.189 μg mL^{-1}. Docking, molecular dynamics, and binding energy calculations suggested that compounds **4** and **5** are promising AChE inhibitors, while compounds **3**, **4**, and **7** are leading candidates against β-secretase. Collectively, this study underscores the potential of *Echinocactus grusonii* as a rich source of bioactive lead compounds for developing novel therapeutics for pharmaceutical applications.

Introduction

Cholinergic neurotransmission is mediated by acetylcholine (ACh), a neurotransmitter that is rapidly hydrolysed after its release by cholinesterase (ChE) enzymes, namely acetylcholinesterase (AChE) and butyrylcholinesterase (BuChE). AChE is localized to the cytoplasm and outer cell membrane of neural synapses and blood cells, as well as throughout the central nervous system (CNS). Each AChE molecule contains an active site with two functional regions, a negatively charged anionic site that binds the positively charged quaternary nitrogen of ACh, and an esteratic site that binds the acyl moiety. This interaction results in the rapid hydrolysis of Ach.[1] Reversible AChE inhibition using compounds containing quaternary or tertiary ammonium functional groups has multiple applications. These include the diagnosis and treatment of various conditions, such as myasthenia gravis, Alzheimer's disease (AD), post-operative ileus, bladder distention, and glaucoma, as well as serving as an antidote for anticholinergic overdose.[1,2]

Beta-site amyloid precursor protein cleaving enzyme 1, commonly known as β-secretase is a key therapeutic target in

Alzheimer's disease (AD) due to its role in formation of amyloid-β (Aβ) plaques, a primary pathological hallmark. Beyond CNS, β-secretase is expressed in other cells such as Schwann cells and is involved in diverse biological processes. For example, its pharmacological inhibition enhances macrophage recruitment and debris clearance in injured nerves, and consequently promotes axonal regeneration.[3,4] Moreover, a significant upregulation of β-secretase was observed in the myocardial tissue of patients with ischemic heart failure.[5] Importantly, the development of drugs targeting β-secretase has been challenging. However, a number of inhibitors have recently entered clinical trials, and their effectiveness in preventing and treating AD has been reported.[6] In recent years, plant-based products have shown promising properties in the treatment of several diseases presenting a valuable source of alternative therapy with high efficacy and fewer side effects.

Cacti are fleshy and pulpy wild-ornamental plants of the family Cactaceae. They grow in dry, semi-arid, and hot climates of South, North and Central America. They are xerophytic plants with great adaptability to harsh environment with economic importance.[7] Cacti plants are cultivated for multiple applications, serving as functional food and livestock fodder. These plants are a valuable source of functional food ingredients, as their consumption provides essential minerals, dietary fiber, phenolic compounds, and various bioactive components.[8]

Echinocactus grusonii Hildm. (Cactaceae) is a xerophyte species widely distributed in the Egyptian ecosystem and is

[a]Department of Pharmacognosy and Medicinal Plants, Faculty of Pharmacy, Al-Azhar University, Cairo, 11884, Egypt. E-mail: ahmedheraiz@gmail.com; ahmedheraiz.2@azhar.edu.eg; ah.othman@azhar.edu.eg

[b]Department of Pharmacognosy, Faculty of Pharmacy, Almaaqal University, Basrah, Iraq
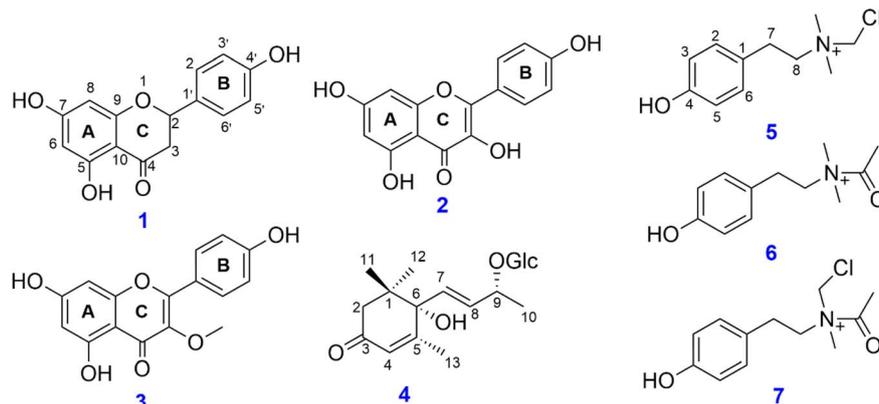
Fig. 1 Structures of the isolated compounds 1–7.

commonly cultivated as an ornamental plant.[9] Previous studies on cactus plants revealed the presence of phenolic compounds, flavonoids, alkaloids and other nitrogenous compounds, betalains, terpenes, and fatty acids.[10]

Given that many species within the Cactaceae family remain unexplored, this study aimed to investigate the chemical constituents of *E. grusonii* and to evaluate their inhibitory activities against AChE and β-secretase. During our search for potential inhibitors of these enzymes from *E. grusonii*, we isolated seven compounds (Fig. 1), including two previously undescribed halogenated amide alkaloids (5 and 7). Herein, we describe the isolation, structural elucidation, and inhibitory activity of these compounds against AChE and β-secretase, highlighting their potential as candidates for central and peripheral nervous system diseases.

Material and methods

Chemicals and standards

β-Secretase inhibitor screening kit (K720-100) and AChE inhibitor screening assay kit (K197-100) were purchased from Bio Vision, USA. Solvents including *n*-hexane, dichloromethane (DCM), ethyl acetate (EtOAc), *n*-butanol (*n*-BuOH), methanol (MeOH), and acetone, were used for extraction and purification (Merck, Darmstadt, Germany). Normal phase-silica gel (0.063–0.200 mm, 70–230 mesh Merck) and a Sephadex LH-20 (Sigma Aldrich, Sweden) were used for open column chromatography. Diaion HP-20 purchased from Mitsubishi Chemical Co., Tokyo, Japan, was used for fractionation. Preparative thin layer chromatography glass plates (PTLC) (20 × 20 cm, silica gel 60 matrix, binder, polymeric, fluorescent indicator (Sigma Aldrich, Sweden) were used for final purification of alkaloids. TLC silica gel 60 F_{254} plates were purchased from Merck, Darmstadt, Germany, and dimethyl sulfoxide (DMSO) was purchased from Cambridge Isotope Laboratories, Andover, MA, USA.

Extraction and isolation

The whole plant *E. grusonii* Hildm. was collected from Helal cactus farm (30°06′29.0″N, 31°06′19.5″E) in July 2023. It was kindly identified by Prof. Abdo Marei Hamed, Professor of Plant Ecology, Botany and Microbiology Department, Faculty of Science, Al-Azhar University, Cairo, Egypt. A voucher specimen EG-2019 was deposited at the herbarium of Pharmacognosy Department, Faculty of Pharmacy, Al-Azhar University, Egypt.

The plant was washed with water, and the roots and spines were removed. The stem was cut into slices and freeze-dried, yielding 1 kg of dried material. This material was then extracted by maceration with 80% aqueous methanol. The extract was concentrated under reduced pressure to yield 100 g of a crude extract. The crude extract was then suspended in H_2O and sequentially partitioned with *n*-hexane, EtOAc, and *n*-BuOH to obtain corresponding fractions of *n*-hexane (1 g), EtOAc (6 g), and *n*-BuOH (25 g). The EtOAc fraction was chromatographed over normal phase-silica gel and eluted with gradient solvent system of DCM–MeOH, to yield 6 subfractions (E_1–E_6). Subfraction E_3 (200 mg) was frequently purified over a Sephadex LH-20 eluted with 100% MeOH to obtain compound 1 (18.0 mg). Compounds 2 (45.0 mg) and 3 (20.0 mg) were obtained from subfraction E_5 (245 mg) by repeated purification steps over a Sephadex LH-20 column eluted with 100% MeOH.

The *n*-BuOH fraction was chromatographed on a Diaion HP-20 column, eluted with a stepwise gradient of H_2O–MeOH, yielding five subfractions (B_1–B_5). Among these, subfraction B_2 was further purified over normal-phase silica gel chromatography using a mixture of DCM–MeOH with 1% ammonia as the eluent, to afford six subfractions (B_{2a}–B_{2f}).

Subfraction B_{2b} was determined as an alkaloid fraction by TLC investigation. It was subsequently purified by repeated chromatography on a Sephadex LH-20 column eluted with 100% MeOH, followed by preparative TLC (DCM–MeOH–NH_4, 80 : 20 : 2, v/v/v), to yield compounds 5 (18.0 mg), 6 (12.0 mg), and 7 (15.0 mg). Additionally, compound 4 (13.0 mg) was isolated from subfraction B_{2c} by repeated Sephadex LH-20 columns eluted with 100% MeOH.

Compound 1: yellow amorphous powder; ^{1}H NMR (400 MHz, DMSO-d_6) δ_H 12.16 (brs, 1H, C-5 OH), 7.32 (d, J = 8.0 Hz, 2H, H-2′, H-6′), 6.81 (d, J = 8.0 Hz, 2H, H-3′/5′), 5.9 (s, 2H, H-6/H-8), 5.45 (dd, J = 13.3 Hz, 1H, H-2), 3.30 (dd, J = 17.0, 12.9 Hz, 1H, H-3$_{ax}$), 2.69 (dd, J = 17.0, 3.0 Hz, 1H, H-3$_{eq}$). ^{13}C NMR (100 MHz, DMSO-d_6) δ_C 196.7 (C-4), 167.7 (C-7), 164 (C-5), 163.4 (C-4′), 158.2 (C-9), 129.4 (C-1′), 128.8 (C-2′/C-6′), 115.6 (C-3′/C-5′), 102.1 (C-10), 96.4

(C-6), 95.6 (C-8), 78.9 (C-2), 42.4 (C-3); HRESIMS m/z 271.0609 [M − H]$^-$ (calcd for $C_{15}H_{11}O_5$, 271.0606), see SI Fig. S1–S3.

Compound **2**: yellow amorphous powder; ^{1}H NMR (400 MHz, DMSO-d_6) δ_H 12.50 (brs, 1H, C-5 OH), 8.06 (d, J = 8.44 Hz, 2H, H-2′/H-6′), 6.94 (d, J = 8.44 Hz, 2H, H-3′/H-5′), 6.45 (s, 1H, H-8), 6.20 (s, 1H, H-6). ^{13}C NMR (100 MHz, DMSO-d_6) δ_C 176.4 (C-4), 164.5 (C-7), 161.2 (C-5), 159.7 (C-4′), 156.6 (C-9), 147.3 (C-2), 136.2 (C-3), 130.0 (C-2′/C-6′), 122.1 (C-1′) 115.9 (C-3′/C-5′), 103.5 (C-10), 98.7 (C-6), 94.0 (C-8); HRESIMS m/z 285.0415 [M − H]$^-$ (calcd for $C_{15}H_9O_6$, 285.0399), see SI Fig. S4–S6.

Compound **3**: yellow amorphous powder; ^{1}H NMR (400 MHz, DMSO-d_6) δ_H 12.69 (brs, 1H, C-5 OH), 7.94 (d, J = 8.8 Hz, 2H, H-2′/H-6′), 6.96 (d, J = 8.8 Hz, 2H, H-3′/H-5′), 6.33 (s, 1H, H-8), 6.11 (s, 1H, H-6), 3.78 (s, 3H, 3-O-CH$_3$). ^{13}C NMR (100 MHz, DMSO-d_6) δ_C 177.9 (C-4), 164.9 (C-7), 161.7 (C-5), 160.7 (C-4′), 157.1 (C-9), 155.6 (C-2), 137.9 (C-3), 130.1 (C-2′/C-6′), 121.1 (C-1′) 116.1 (C-3′/C-5′), 103.8 (C-10), 99.8 (C-6), 94.5 (C-8), 60.2 (3-O-CH$_3$); HRESIMS m/z 299.0507 [M − H]$^-$ (calcd for $C_{16}H_{11}O_6$, 299.0556), see SI Fig. S7–S9.

Compound **4**: yellow amorphous powder; ^{1}H NMR (400 MHz, DMSO-d_6) δ_H 5.99 (d, J = 15.44 Hz, 1H, H-7), 5.78 (s, 1H, H-5), 5.69 (dd, J = 15.88, 6.32 Hz, 1H, H-8), 4.46 (m, 1H, H-9), 4.12 (d, J = 7.72 Hz, 1H, H-1′), 2.9–3.8 (6H, (H-2′/H-6′)), 1.83 (s, 3H, CH$_3$-13), 2.59 (d, J = 16.68 Hz, 1H, H-2$_{ax}$), 2.09 (d, J = 16.68 Hz, 1H, H-2$_{eq}$), 1.21 (d, J = 6.44 Hz, 3H, CH$_3$-10), 0.94 (s, 3H, CH$_3$-12), 0.93 (s, 3H, CH$_3$-11). ^{13}C NMR (100 MHz, DMSO-d_6) δ_C 197.9 (C-3), 164.3 (C-5), 132.1 (C-7), 131.9 (C-8), 126.0 (C-4), 100.4 (C-1′), 78.4 (C-6), 77.5 (C-5′), 73.8 (C-3′), 73.7 (C-9), 72.4 (C-2′), 70.5 (C-4′), 61.5 (C-6′), 49.8 (C-2), 41.4 (C-1), 24.6 (C-11), 23.6 (C-12), 22.5 (C-10), 19.1 (C-13); ESIMS m/z 387 [M + H]$^+$, see SI Fig. S10–S12.

Compound **5**: colourless needle crystals; ^{1}H NMR (400 MHz, DMSO-d_6) δ_H 7.12 (d, J = 8.44 Hz, 2H, H-2/H-6), 6.78 (d, J = 8.44 Hz, 2H, H-3/H-5), 5.50 (s, 2H, N-CH$_2$Cl), 3.39 (s, 6H, 2N-CH$_3$), 3.62 (dd, J = 15.44, 6.32 Hz, 2H, H-8), 2.96 (t, J = 15.44 Hz, 2H, H-7). ^{13}C NMR (100 MHz, DMSO-d_6) δ_C 157.0 (C-4), 130.4 (C-2/C-6), 126.0 (C-1), 116.0 (C-3/C-5), 68.7 (N-CH$_2$Cl), 63.6 (C-8), 49.3 (2N-CH$_3$), 27.6 (C-7); HRESIMS m/z 214.0996 [M]$^+$ (calcd for $C_{11}H_{17}ClNO^+$, 214.0993), see SI Fig. S13–S18.

Compound **6**: colourless needle crystals; ^{1}H NMR (400 MHz, DMSO-d_6) δ_H 9.18 (brs, 1H, C-1 OH), 7.02 (d, J = 8.4 Hz, 2H, H-2/H-6), 6.68 (d, J = 8.4 Hz, 2H, H-3/H-5), 2.63 (brt, 2H, H-7), 2.48 (brt, 2H, H-8), 2.23 (s, 6H, 2N-CH$_3$), 1.9 (s, 3H, CO-CH$_3$). ^{13}C NMR (100 MHz, DMSO-d_6) δ_C 172.7 (N-CO), 155.9 (C-4), 129.9 (C-2/C-6), 126.0 (C-1), 115.5 (C-3/C-5), 61.5 (C-8), 45.3 (2N-CH$_3$), 32.7 (C-7), 21.7 (CO-CH$_3$); HRESIMS m/z 208.1348 [M]$^+$, see SI Fig. S19–S23.

Compound **7**: colourless needle crystals; ^{1}H NMR (400 MHz, DMSO-d_6) δ_H 7.12 (d, J = 8.44 Hz, 2H, H-2/H-6), 6.78 (d, J = 8.44 Hz, 2H, H-3/H-5), 5.50 (s, 2H, N-CH$_2$Cl), 3.62 (dd, J = 15.44, 6.32 Hz, 2H, H-8), 3.26 (s, 3H, NCH$_3$), 2.96 (t, J = 15.44 Hz, 2H, H-7), 1.78 (s, 3H, NCH$_3$). ^{13}C NMR (100 MHz, DMSO-d_6) δ_C 177.1 (N-CO), 157.0 (C-4), 130.4 (C-2/C-6), 126.0 (C-1), 116.0 (C-3/C-5), 68.7 (N-CH$_2$Cl), 63.5 (C-8), 49.3 (NCH$_3$), 27.7 (C-7), 24.3 (CO-CH$_3$); HRESIMS m/z 242.0975 [M]$^+$ (calcd for $C_{12}H_{17}ClNO_2^+$, 242.0942), see SI Fig. S24–S29.

Identification of the isolated compounds

The NMR spectra for the isolated compounds were recorded on Bruker DRX-400 spectrometer (Bruker Daltonics, Billerica MA, USA) utilizing tetramethyl silane (TMS) as an internal standard. The chemical shift was expressed as δ values. HR-MS of compounds was determined using a quadrupole time-of-flight (q-tof) mass spectrometer (Agilent Technologies, USA). Also, ESI-MS positive and negative ion acquisition mode was carried out on a XEVO TQD triple quadruple instrument (Waters Corporation, USA).

In vitro enzyme assays

***In vitro* β-secretase inhibition assay.** A β-secretase inhibitory assay was performed using a BACE Inhibitor Screening Assay Kit, Bio Vision, USA; K720-100, following the manufacturer's protocol and the method described by.[11] Briefly, the isolated compounds and control samples (solvent, inhibitor, and enzyme) were prepared. Then, 50 μL of each were aliquoted into the designated wells of a microplate. Subsequently, 2 μL of diluted β-secretase enzyme was added to each well, followed by incubation for 5 minutes at 25 °C. Then, 50 μL of substrate solution was added to each well, and the plate was shaken gently to mix. The fluorescence intensity was measured. Curcumin was used as a positive standard at the same test concentrations. The inhibition percentage was calculated using the following equation:

$$\% \text{ Relative inhibition} = \frac{\text{slope of EC} - \text{slope of S}}{\text{slope of EC}} \times 100$$

where, slope of EC is the slope of the enzyme control, and slope of S is the slope of tested sample.

***In vitro* acetylcholinesterase (AChE) inhibition assay.** The AChE inhibition assay was performed using a commercial kit, AChE Inhibition Screening Kit, Bio Vision, K197-100, according to the manufacturer's protocol. Briefly, 10 μL of diluted AChE enzyme was added to wells containing the test sample [S], inhibitor control [IC], solvent control [SC], and enzyme control [EC]. Subsequently, 10 μL of AChE assay buffer was added to the well designated as background control [BC]. The volume in all wells was then adjusted to 160 μL per well using AChE assay buffer. The plate was mixed thoroughly and incubated at room temperature for 10–15 minutes, protected from light. Following that, 40 μL of a freshly prepared reaction mix, comprising diluted AChE substrate (10 μL), probe mix (5 μL), and AChE assay buffer (25 μL), was added to all wells. The plate was mixed thoroughly, resulting in a final reaction volume of 200 μL per well. The absorbance was measured at 412 nm in kinetic mode for 40 minutes at room temperature. Donepezil was used as a positive drug. The inhibition percentage was calculated using the relative inhibition equation previously described.

Docking-based virtual screening

Ligand structure generation. OpenBabel v.3.1.1 (ref. 12) was used to convert the structures' SMILE codes to three-dimensional configurations that were subsequently subjected to a minimization of energy using the steepest descent

technique with the same software. The minimization was performed by the force field MMFF94. Using AutoDockTools v.4.2, all torsions of the selected structures were assigned and their Gasteiger charges were provided for all studied atoms in structures.[13]

Protein structure preparation. For docking screening, the human AChE and β-secretase crystal structures (PDB codes: 4W93 and 3L4W, respectively)[14,15] were used. PDBfixer[16] was used to edit the downloaded structure, adding missing residues and atoms, and removing co-crystalized H_2O and heteroatoms. Through AutoDockTools v.4.2, polar hydrogen and Gasteiger charges were subsequently made available for both proteins.

Structural docking. The docking process was carried out using the PyRx platform's built-in AutoDock Vina software.[16,17] According to the co-crystalized ligands of both enzymes, the docking search grid boxes were determined to perfectly enclose them with a 20 Å3 total size.

The grid box's coordinates were set to be $x = -9.682$; $y = 4.274$; $z = -23.145$ and $x = 45.424$; $y = 92.375$; $z = 34.811$, respectively. The level of exhaustion was held at 24. Pymol software was used to evaluate and display docking poses. Exhaustiveness was set to 24. Ten poses were generated for each docking experiment. Docking poses were analysed and visualized using Pymol software.[18] The docking protocol was validated by re-docking the co-crystalized ligands into the active sites of both enzymes. The resulting top-scoring poses of both ligands were in good alignment with the co-crystalized ones with slight deviations (RMSDs = 1.27 and 1.04, respectively).

Molecular dynamics simulation

MD simulations were conducted using NAMD 3.0.0 software,[19] which applies the Charmm-36 force field. Protein systems were constructed using the QwikMD toolkit of VMD software,[20] ensuring the protein structures had no missing hydrogens, setting the protonation states of the amino acid residues to pH 7.4, and removing co-crystallized water molecules. The structures were then embedded in an orthorhombic box of TIP3P water with 0.15 M Na^+ and Cl^- ions in a 20 Å solvent buffer. The systems were energy minimized and equilibrated for 5 nanoseconds. The parameters and topologies of the ligands were calculated using the VMD plugin Force Field Toolkit (ffTK). These generated parameters and topology files were loaded into VMD[21] to read the protein–ligand complexes accurately and conduct the simulation steps.

Binding free energy calculations

Molecular Mechanics Poisson–Boltzmann Surface Area (MM-PBSA) embedded in the MMPBSA.py module of AMBER18 was utilized to calculate the binding free energy of the docked complex.[22] 100 frames were processed from the trajectories in total, and the system's net energy was estimated using the following equation:

$$\Delta G_{binding} = \Delta G_{complex} - \Delta G_{receptor} - \Delta G_{inhibitor}$$

Each of the afore mentioned terms requires the calculation of multiple energy components, including van der Waals energy, electrostatic energy, internal energy from molecular mechanics, and polar contribution to solvation energy.

Statistical analysis

To obtain the experimental results in this study, all experimental studies were carried out in triplicate manner, and the results are expressed as the means ± SD ($n = 3$). The statistical significance of differences between means was established using ANOVA with Duncan's *post hoc* tests. p values < 0.05 indicate statistical significance.

Results and discussion

Identification of the isolated compounds

Compound **1** was obtained as a yellowish-white amorphous powder. Its molecular formula was determined as $C_{15}H_{12}O_5$ from the negative ESIMS data at m/z 271.0609 $[M - H]^-$. The ^1H NMR spectrum of **1** revealed two doublet proton signals, each integrating for two protons resonating at δ_H 7.32 (d, $J = 8.0$ Hz) and 6.81 (d, $J = 8.0$ Hz) indicating the presence of two *ortho*-coupled equivalent pairs of protons H-2′/6′ and H-3′/5′, respectively, resembling typical AA′BB′ pattern of 1,4-disubstituted B ring of flavonoids. Additionally, the presence of a singlet proton signal integrating for two protons at δ_H 5.91 gives insights on the characteristically overlapped A ring protons H-6 and H-8 of flavanones.[23] Besides, the ring C of **1** was determined as a flavanone, with three doublet of doublet signals at δ_H 5.45 (H-2, $J = 3.0$, 13.0 Hz), 2.69 (H-3$_{eq}$, $J = 17.0$, 3.0 Hz), and 3.30 (H-3$_{ax}$, $J = 17.0$, 12.9 Hz).[24] On the other hand, the APT NMR spectrum confirmed the previously elucidated structure with 13 carbon signals. Comparison of APT NMR spectroscopic data of **1** with those previously reported, indicated signals resonating at δ_C 78.9, 42.4 and 196.7, that were assigned for C-2, C-3, and C-4, respectively, further confirmed flavanone skeleton.[25] Moreover, the existence of two carbon signals at δ_C 96.4 and 95.6 with approximate difference value of δ 1 ppm confirmed C-6 and C-8 of ring A.[26] Additional carbon signals at δ_C 115.6 and 128.8 further confirmed the substitution pattern of ring B *i.e.*, 1,4 disubstituted.[24] Compound **1** was thus elucidated as naringenin.

Compound **2** was obtained as a yellow amorphous powder, and its molecular formula was established as $C_{15}H_{10}O_6$ by a molecular ion peak in ESI-MS analysis at m/z 285.0415 $[M - H]^-$. The NMR data were consistent with those reported in literature.[27,28] The flavonoid ring B was determined by two doublets (AA′BB′ system), each integrating for two protons, resonating at δ_H 8.06 for H-2′/H-6′ ($J = 8.4$ Hz) and 6.94 for H-3′/H-5′ ($J = 8.4$ Hz), indicating a 1,4-disubstituted ring. Additionally, two broad singlet signals at δ_H 6.19 and 6.44 were assigned for H-6 and H-8 in ring A.[27] About APT NMR analysis, 13 carbon signals were detected. Among them, a characteristic signal at δ_C 176.4 (C-4) was assigned for a carbonyl group indicating a flavonol. The flavonoid ring A was further confirmed by signals at δ_C 98.7 and 94.0 assigned for C-6 and C-8, respectively.

Whilst a 1,4-disubstituted ring B was confirmed by the presence of two carbon signals at δ_C 115.9 and 130.0 revealing C-3′/C-5′ and C-2′/C-6′, respectively.[28,29] Hence, compound **2** was elucidated as 3,4′,5,7-tetrahydroxyflavone, commonly known as kaempferol.

Compound **3** was obtained as a yellowish-white amorphous powder. The negative mode of ESIMS analysis of **3** revealed a molecular ion peak at m/z 299.0507 [M − H]⁻, and the molecular formula was determined to be $C_{16}H_{12}O_6$. The ¹H NMR spectrum showed two doublet proton signals, each with two proton integrations, at δ_H 7.94 (J = 8.8 Hz) and 6.96 (J = 8.8 Hz) indicating the presence of two *ortho*-coupled equivalent pairs of H-2′/6′ and H-3′/5′, respectively, resembling typical AA′BB′ pattern of 1,4-disubstituted B ring of flavonoids. Besides, the presence of two broad singlet proton signals at δ 6.33 and 6.11 were assigned for H-6 and H-8 of ring A. The presence of a methoxy group in the flavonoid structure was characterized by a singlet signal at δ 3.78 (3H).[28] Moreover, the APT NMR spectrum revealed 13 carbon signals. Among them, a characteristic signal at δ_C 177.9 (C-4) indicated a carbonyl group in the flavonoid structure.[29] The APT NMR data were similar to those reported for **2** except for an additional methoxyl group in **3**, which was confirmed by carbon signal at δ_C 60.2.[26] In contrast to **2**, the attachment of C-3 methoxyl group was deduced from the downfield shifts of C-2 (δ_C 155.6), C-3 (δ_C 137.9) and C-4 (δ_C 177.9).[26,28] Hence, compound **3** was identified as 3-methoxy kaempferol.

Compound **4** was isolated as a yellow amorphous powder with a molecular formula of $C_{19}H_{30}O_8$. For aglycone part, the ¹H NMR spectrum of **4** showed two *trans*-olefinic proton signals at δ_H 5.99 (H-7, d, J = 15.44 Hz) and δ_H 5.69 (H-8, dd, J = 15.88, 6.32 Hz). Additionally, a broad singlet vinyl proton signal at δ_H 5.78 was assigned for H-4. Besides, a multiplet signal observed at δ_H 4.46 revealed an oxymethine proton at C-9. Furthermore, two geminal methylene protons at C-2 were assigned at δ_H 2.09 (H-2a, J = 16.68 Hz), 2.59 (H-2b, J = 16.68 Hz). Three singlet methyl signals resonated at δ_H 0.93, 0.94 and 1.83 were assigned for C-11, C-12 and C-13, respectively. The presence of a doublet signal at δ_H 1.21 (J = 6.44 Hz) indicated an additional methyl group at C-10. These data suggested that **4** is a C13 megastigmane (α-dihydro-ionyl type) derivative.[30,31] For sugar part, a typical set of signals due to a β-glucosyl moiety was observed at δ_H (4.12, d, J = 7.72 Hz) assigned for anomeric proton at C-1′. Besides, signals resonated at δ_H 2.9–3.8 were assigned for the remaining sugar protons.[32] The APT NMR data revealed 19 carbon signals, including 6 sugar carbon signals at δ_C 100.4 (C-1′), 77.5 (C-5′), 73.8 (C-3′), 72.4 (C-2′), 70.5 (C-4′), and 61.5 (C-6′). The remaining 13 signals were assigned for the aglycone moiety, with four quaternary carbons appearing at δ_C 197.9 (C-3, carbonyl), 164.3 (C-5), 78.4 (C-6), and 41.4 (C-1). Additionally, three olefinic carbons were observed at δ_C 126.0 (C-4), 132.1 (C-7), and 131.9 (C-8), while a hydroxylated methine (C-9) resonated at δ_C 73.7. A methylene carbon (C-2) appeared at δ_C 49.8, and four methyl groups were identified at δ_C 24.6 (C-11), 23.6 (C-12), 22.5 (C-10), and 19.1 (C-13). Based on NMR data and comparison with literature, compound **4** was identified as vomifoliol-9-O-β-D-glucopyranoside.[32,33]

Compound **5** was isolated as colourless needles and gave a positive orange-red reaction with Dragendorff's reagent,

suggesting a nitrogen-containing alkaloid. High-resolution mass spectrometry (HRESIMS) established the molecular formula as $C_{11}H_{17}ClNO^+$, based on the [M]⁺ ion at m/z 214.0996. The characteristic 3:1 isotopic ratio of the [M]⁺ and [M + 2]⁺ peaks confirmed the presence of a single chlorine atom.[34–36] The ¹H NMR spectrum provided significant structural insight. Signals for a 1,4-disubstituted benzene ring [δ_H 7.12 (d, J = 8.44 Hz) and 6.78 (d, J = 8.44 Hz)] and an ethyl side chain [δ_H 2.96 (H₂-7), 3.62 (H₂-8)] were determined in the structure of **5**. A singlet signal with six protons at δ_H 3.39 indicated the presence of an *N,N*-dimethyl groups. Together, these features suggested that compound **5** was a derivative of the known compound hordenine.[37] However, a key difference was a distinct downfield-shifted singlet at δ_H 5.5, integrating for two protons. The deshielding of this methylene group was consistent with its attachment to both a nitrogen and an electronegative chlorine atom, suggesting a –CH₂Cl moiety.[35] The ¹³C NMR showed a resonance at δ_C 68.7 was characteristic for a methylene group bonded to chlorine. The remaining carbon signals [δ_C 157.0 (C-4), 130.4 (C-2/C-6), 126.0 (C-1), 116.0 (C-3/C-5), 63.6 (C-8), 49.3 (2N-CH₃), 27.6 (C-7)] were fully consistent with the hordenine skeleton.

The final structure was confirmed by 2D NMR experiments. Key evidence included a COSY spectrum revealing the spin systems of the ethyl side chain (H₂-7/H₂-8) and the aromatic ring (H-2/6 with H-3/5). Moreover, HMBC correlations of chloro-methylene protons (δ_H 5.5) to *N*-methyl carbons (δ_C 49.3) and C-8 (δ_C 63.6) confirmed the presence of –CH₂Cl group directly on the nitrogen atom. Additional HMBC correlations from the *N*-methyl protons to H₂-7 and H₂-8 further confirmed the structure (Fig. 2). Therefore, based on spectroscopic evidence—including MS, ¹H NMR, ¹³C NMR, HSQC, HMBC, and COSY—compound **5** was identified as *N*-chloromethyl hordenine.

Compound **6**, with molecular formula ($C_{12}H_{18}NO_2^+$), was obtained as colourless needles and gave an orange-red spot when sprayed with Dragendorff's reagent indicating its possible nitrogenous or alkaloidal nature. Its spectroscopic data (¹H and APT NMR) were similar to those reported in the literature for *N*-acetyl hordenine,[37,38] confirming its structure.

Compound **7** was isolated as colourless needles and produced an orange-red spot with Dragendorff's reagent, indicating its alkaloidal nature. High-resolution mass spectrometry (HRESIMS) indicated the molecular formula as $C_{12}H_{17}ClNO_2^+$, based on the [M]⁺ ion peak at m/z 242.0975. Analysis of the NMR data revealed that compound **7** shared a core structure with compound **5**. This was evidenced by the signals for a 1,4-disubstituted benzene ring [δ_H 7.12, 6.78 (each 2H, d, J = 8.44 Hz); δ_C 157.0 (C-4), 130.4 (C-2/C-6), 126.0 (C-1), 116.0 (C-3/C-5)], an ethylamine side chain [δ_H 2.96 (H₂-7), 3.64 (H₂-8); δ_C 27.6 (C-7), 63.5 (C-8)], an *N*-methyl
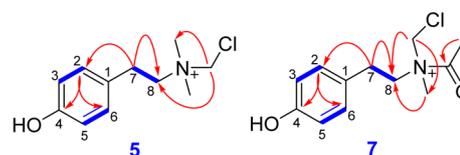

Fig. 2 Key HMBC ⌢ and COSY ▬ correlations of compounds **5** and **7**.

group [δ_H 3.26 (3H, s); δ_C 49.3], and the characteristic N-chloromethyl group [δ_H 5.5 (2H, s); δ_C 68.7].

The key structural distinction was the presence of an acetyl group in compound **7**, indicated by a methyl signal at δ_H 1.78 (3H)/δ_C 24.3, and a corresponding carbonyl carbon at δ_C 177.1. The presence of this acetyl group was confirmed by HMBC spectroscopy, which showed a key correlation from the acetyl methyl protons (δ_H 1.78) to the carbonyl carbon (δ_C 177.1). This, combined with the molecular formula requiring two additional atoms (C and O) beyond the structure of compound **5**, definitively established the N-acetyl substitution. The structure was further confirmed by 2D NMR experiments. The COSY spectrum confirmed the spin systems of the ethyl side chain (H_2-7/H_2-8) and the aromatic ring. The HMBC spectrum demonstrated correlations of N-methyl and N-chloromethyl protons to C-8, as well as correlations of H_2-7 to both C-8 and the aromatic carbons C-2/C-6 (Fig. 2). Hence, based on these spectroscopic data, compound **7** was identified as N-acetyl-N-chloromethyl-N-methyl tyramine.

Inhibitory effects on β-secretase

According to previous reports, β-secretase enzyme plays an important role in amyloid beta (Aβ) deposition, which results in long-term cognitive decline and is a major factor in AD.[3,11] The ability of compounds obtained from *E. grusonii* to inhibit β-secretase was assessed, and the results are depicted in Table 1. The results revealed a promising activity of all tested compounds with IC_{50} values less than 2 μg mL^{-1}, except for compound **2**. Moreover, the results revealed potent activity of compounds **1**, **3**, and **4** with IC_{50} values of 0.422 ± 0.014, 0.134 ± 0.003, and 0.066 ± 0.002 μg mL^{-1}, respectively, as compared with curcumin with an IC_{50} 0.272 ± 0.009 μg mL^{-1}. The higher activity of **1** compared to **2** suggests that the flavanone moiety is important for activity, unlike the flavonol structure in **2** (IC_{50} = 7.189 ± 0.237 μg mL^{-1}).

Additionally, the alkaloid derivatives **5** and **7** demonstrated potent inhibitory activity, with IC_{50} values of 0.268 ± 0.009 and 0.12 ± 0.004 μg mL^{-1}, respectively. These values were significantly lower than that of compound **6**, suggesting that the presence of a halogen moiety is crucial for the observed activity.

Inhibitory effects on AChE

Acetylcholinesterase (AChE) is a key enzyme in the central and peripheral nervous systems, responsible for catalysing the

hydrolysis of acetylcholine in cholinergic synapses. Consequently, acetylcholinesterase inhibitors (AChEIs) can modulate critical pathogenic pathways.[39] Based on this rationale, the isolated compounds were evaluated for their AChE inhibitory activity.

The results showed dose dependent inhibition activity of compounds toward AChE as seen in Table 1. In the current study, compound **1** revealed a potent AChE inhibition with an IC_{50} value of 0.212 ± 0.007 μg mL^{-1}. This finding aligns with the reported *in vitro* and *in silico* AChE inhibitory activity of naringenin and its derivatives.[40] The potent activity of **1** (IC_{50} = 0.212 ± 0.007 μg mL^{-1}) compared to **3** (IC_{50} = 1.099 ± 0.03 μg mL^{-1}) suggests that the flavanone moiety is critical for activity, unlike the flavonol structure in **2**. On the other hand, a m-ethoxylated flavonol, compound **3**, showed better activity than **2**, with IC_{50} = 0.483 ± 0.015 μg mL^{-1}. Importantly, the alkaloid derivative, compound **5**, demonstrated the most promising anti-AChE activity (IC_{50} = 0.076 ± 0.002 μg mL^{-1}), which was stronger than that of all other tested compounds and the reference drug, donepezil (IC_{50} = 0.171 ± 0.005 μg mL^{-1}). Moreover, the other halogenated alkaloid derivative, compound **7**, exhibited a remarkable anti-AChE activity with an IC_{50} value of 0.607 ± 0.02 μg mL^{-1}. In contrast, compound **6** showed a moderate activity with an IC_{50} value = 2.255 ± 0.074 μg mL^{-1}.

These findings highlight the critical role of the chlorine moiety in enhancing anti-AChE activity, potentially due to the increased lipophilicity provided by the chlorine atom.[39] Consequently, the isolated secondary metabolites, particularly the halogenated alkaloids from *E. grusonii*, emerge as promising candidates for developing therapies for conditions including myasthenia gravis, glaucoma, and post-operative ileus.

In silico studies and dynamic simulations

In silico screening using AutoDock Vina yielded predicted binding affinities spanning from −6.5 to −8.9 kcal mol^{-1} for human AChE and from −6.2 to −9.0 for human β-secretase (Table 2). N-Chloromethyl hordenine (**5**) ranked the top-scoring compound against AChE, while isokaempferide (**3**) ranked the top-scoring compound against β-secretase.

The docking scores showed a good correlation with the *in vitro* activities against AChE (R^2 = 0.78). Compounds such as N-chloromethyl hordenine **5** and vomifoliol-9-O-β-D-glucopyranoside **4**, both of which displayed low IC_{50} values, ranked among

Table 1 Inhibitory activities of compounds (IC_{50}) against acetylcholinesterase (AChE) and β-secretase enzymes. All values are expressed in μg mL^{-1} ± SD of three independent experiments

Compound	AChE (μg mL^{-1} ± SD)	β-Secretase (μg mL^{-1} ± SD)
Naringenin **1**	0.212 ± 0.007	0.422 ± 0.014
Kaempferol **2**	1.099 ± 0.03	7.189 ± 0.237
Isokaempferide **3**	0.483 ± 0.015	0.134 ± 0.003
Vomifoliol-9-O-β-D-glucopyranoside **4**	0.452 ± 0.014	0.066 ± 0.002
N-Chloromethyl hordenine **5**	0.076 ± 0.002	0.268 ± 0.009
N-Acetyl hordenine **6**	2.255 ± 0.074	1.711 ± 0.056
N-Acetyl-N-chloromethyl-N-methyl tyramine **7**	0.607 ± 0.02	0.12 ± 0.004
Donepezil	0.171 ± 0.005	—
Curcumin	—	0.272 ± 0.009

Table 2 Docking scores (in kcal mol^{-1}) of the tested compounds against human acetylcholinesterase (AChE) and β-secretase using AutoDock Vina

Compound	AChE	β-Secretase
Naringenin **1**	−8.0	−7.5
Kaempferol **2**	−7.0	−6.2
Isokaempferide **3**	−8.4	**−9.0**
Vomifoliol-9-*O*-β-D-glucopyranoside **4**	−8.5	−8.8
N-Chloromethyl hordenine **5**	**−8.9**	−8.7
N-Acetyl hordenine **6**	−6.5	−7.1
N-Acetyl-*N*-chloromethyl-*N*-methyl tyramine **7**	−8.2	−8.9
Donepezil	−9.4	—
Curcumin	—	−8.6

the top docking hits (−8.9 and −8.5 kcal mol^{-1}, respectively). This close agreement between the computational and experimental data indicates that AutoDock Vina provided a reliable ranking of ligands for AChE, which is consistent with the well-defined and structurally rigid binding gorge of the enzyme.

For β-secretase, the correlation was more modest ($R^2 = 0.62$). Potent inhibitors such as isokaempferide **3** and *N*-acetyl-*N*-chloromethyl-*N*-methyl tyramine **7** achieved highly favourable docking scores (−9.0 and −8.9 kcal mol^{-1}), which matched well with their experimental potencies. Some deviations were observed; for example, *N*-acetyl hordenine **6** exhibited relatively weak inhibition *in vitro* yet was predicted to bind with a moderately favourable score (−7.1 kcal mol^{-1}). Such discrepancies are expected given the flexible, solvent-exposed active site of β-secretase, which is challenging to capture fully with rigid docking.

Taken together, both docking and experimental data highlighted *N*-chloromethyl hordenine **5** and vomifoliol-9-*O*-β-D-glucopyranoside **4** as the most promising AChE inhibitors,

whereas isokaempferide **3** and *N*-acetyl-*N*-chloromethyl-*N*-methyl tyramine **7** emerged as the leading candidates against β-secretase. On this basis, the best-scoring compound for each enzyme was advanced to molecular dynamics (MD) simulations and absolute binding free energy calculations in order to evaluate the stability and energetics of the ligand–enzyme complexes under dynamic conditions.

Compound **5** (Fig. 3A) was stabilized primarily through a strong π–cation interaction with Tyr-337, a key residue responsible for recognition of cationic moieties, as well as a hydrogen bond with Tyr-133 and an electrostatic contact with Asp-74 at the peripheral anionic site. Additional hydrophobic stabilization was contributed by Trp-86, Phe-338, and Tyr-341. In contrast, compound **7** (Fig. 3B) retained the conserved π–cation interaction with Tyr-337 and a hydrogen bond with Tyr-133, but it lacked the electrostatic interaction with Asp-74, which reduced its anchoring capacity. Its stabilization was therefore mainly dependent on aromatic stacking with Trp-86 and surrounding hydrophobic residues. The co-crystallized inhibitor (Fig. 3C) displayed the canonical π–cation contact with Tyr-337, along with hydrogen bonding to Phe-295, and strong hydrophobic packing with Trp-86, Tyr-124, Phe-297, and Phe-338.

RMSD analysis across 200 ns (Fig. 3D) showed that compound **5** maintained the most stable trajectory, equilibrating after ~30 ns and remaining within 1.5–2.0 Å. The co-crystallized ligand exhibited slightly lower fluctuations (1.2–1.6 Å) consistent with its crystallographically validated pose. By contrast, compound **7** displayed less stability, with RMSD values frequently deviating beyond 2.0 Å and larger fluctuations over the course of the simulation, reflecting its weaker anchoring within the active site.

The MM/PBSA free energy estimates supported these observations, giving binding energies of −9.6 kcal mol^{-1} for compound
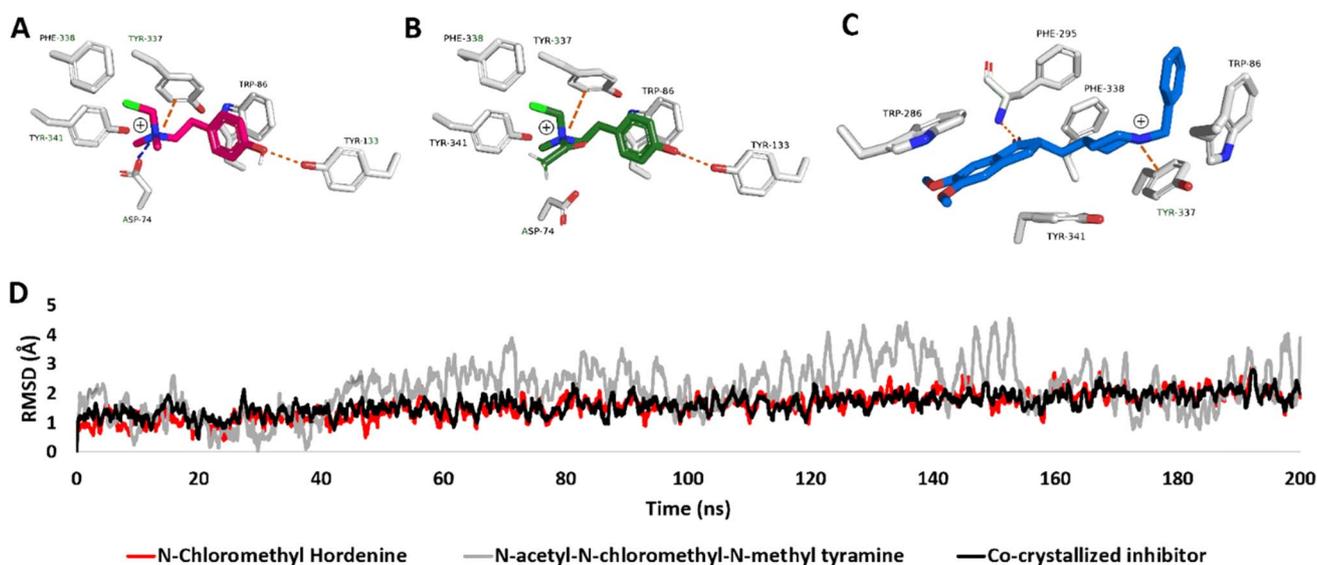

Fig. 3 The most populated binding pose of compound **5** (*N*-chloromethyl hordenine) and **7** (*N*-acetyl-*N*-chloromethyl-*N*-methyl tyramine) extracted from the equilibrated MD trajectory (A and B, respectively) within the active site of human acetylcholinesterase (AChE) compared to the co-crystallized inhibitor (C). (D) Root-mean-square deviation (RMSD) profiles of compound **5**, **7** and the co-crystallized inhibitor over a 200 ns simulation.

5, −7.7 kcal mol^{-1} for compound 7, and −9.1 kcal mol^{-1} for the reference ligand. This confirmed that compound 7 binds favorably but with reduced stability and affinity compared to compound 5 and the co-crystallized inhibitor.

MD simulations of isokaempferide 3, *N*-acetyl-*N*-chloromethyl-*N*-methyl tyramine 7, and the co-crystallized inhibitor in β-secretase revealed distinct binding modes.

Compound 3 (Fig. 4A) established a well-defined binding pose, forming hydrogen bonds with Gly-74, Tyr-198, and Asp-228, securely anchoring its flavonoid scaffold. Compound 7 (Fig. 4B) engaged fewer contacts, primarily a hydrogen bond with Gly-74 and additional polar stabilization from Asp-228 but did not form extensive anchoring interactions. The co-crystallized inhibitor (Fig. 4C) displayed the expected triad of hydrogen bonds with Asp-32, Gly-230, and Asp-228, together with stabilization by Trp-115.

The RMSD trajectories over 200 ns (Fig. 4D) confirmed that compound 3 equilibrated early and maintained RMSD values between 1.5–2.2 Å, indicating stable binding. The co-crystallized inhibitor was slightly more rigid (1.2–1.8 Å), while compound 7 showed greater fluctuations (1.7–2.8 Å), consistent with a more flexible and less stable pose.

Binding free energy calculations echoed these findings, with MM/PBSA values of −8.3 kcal mol^{-1} for compound 3, −7.3 kcal mol^{-1} for compound 7, and −8.4 kcal mol^{-1} for the co-crystallized inhibitor. This suggest networks while compound 7 retains favourable binding to β-secretase, its stability and interaction network are weaker than those of compound 3 and the reference ligand.

Chemotaxonomic significance of alkaloids in Cactaceae

The Cactaceae family is a well-known source of diverse alkaloids, primarily phenethylamines and 1,2,3,4-tetrahydroisoquinolines, as comprehensively reviewed by Cassels and colleagues in 2019.[41] Within this chemotaxonomic framework, simple phenethylamines such as hordenine, mescaline, *N*-methyl mescaline, and candicine are recognized as classic and widespread constituents. Moreover, numerous isoquinoline alkaloids, including anhalamine, anhalonidine, pellotine, and lophophorine, have also been consistently identified. These alkaloids are most prevalent in the Cactoideae subfamily, with fewer occurrences reported in the Opuntioideae and Pereskioideae.

In our study, the isolated hordenine derivatives from *Echinocactus grusonii* fit this established phytochemical profile, reinforcing shared biosynthetic pathways within the Cactoideae. Of particular significance is the discovery of two rare, halogenated alkaloids classified as chlorinated hordenine derivatives. To the best of our knowledge, the presence of a chlorine atom in this class of cactus alkaloids is exceptionally rare, with no previous reports of such analogs within the Cactaceae family. This finding significantly expands the known
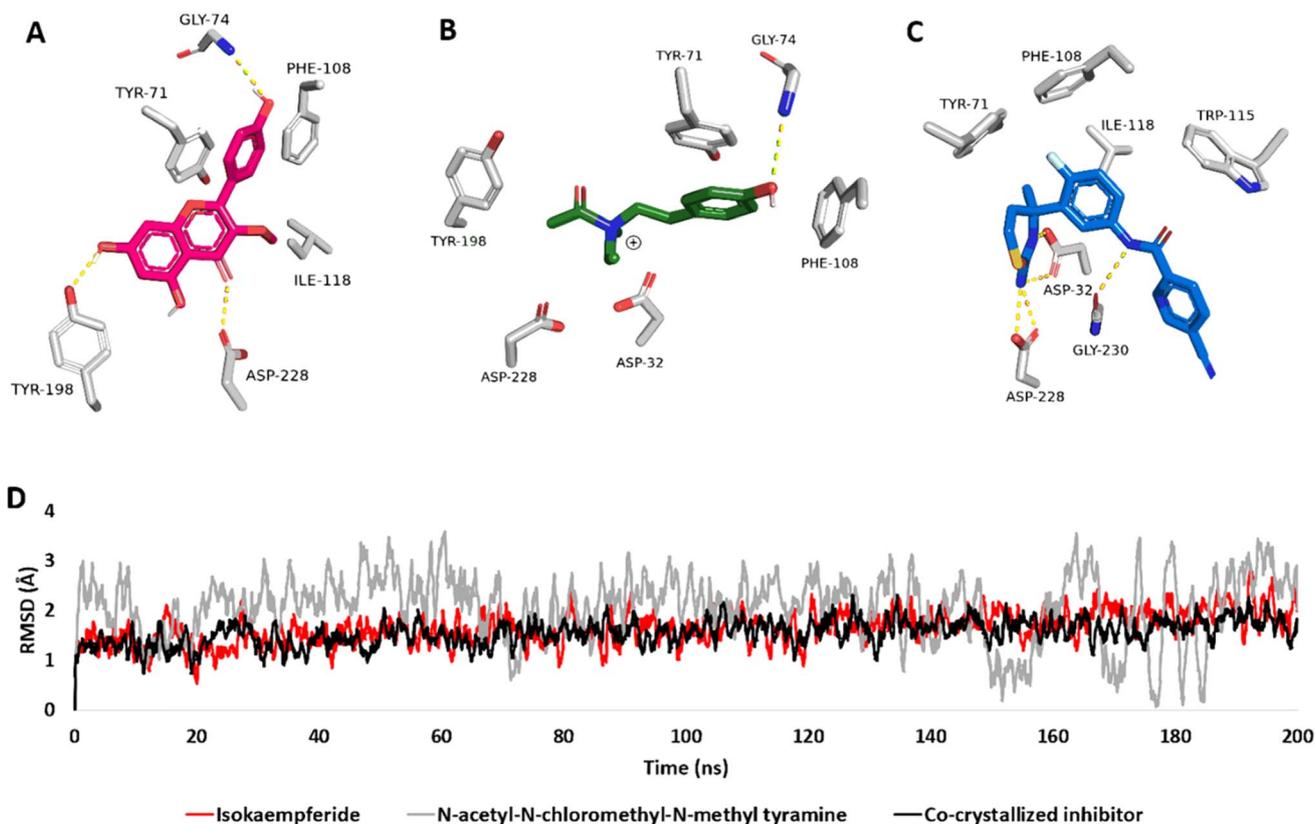

Fig. 4 The most populated binding pose of compound 3 (isokaempferide) and 7 (*N*-acetyl-*N*-chloromethyl-*N*-methyl tyramine) (A and B, respectively) compared to the binding pose of the co-crystallized inhibitor (C). (D) Root-mean-square deviation (RMSD) profiles of both ligands together with the co-crystallized inhibitor over a 200 ns simulation.

chemical diversity of alkaloids in this family and suggests a unique halogenation capability in *E. grusonii*. Therefore, this work not only corroborates the expected alkaloid chemistry but also highlights *E. grusonii* as a promising source of novel natural products, underscoring the importance of investigating even well-known plant families.

Conclusion

The present study deals with the isolation and structural characterization of seven compounds from the stem part of *E. grusonii* Hildm. The potential inhibitory activity of the isolated compounds against β-secretase and AChE enzymes was evaluated. Almost all isolated compounds revealed promising inhibition activity against targeted enzymes, β-secretase and AChE. Interestingly, the study revealed promising activity of alkaloid derivatives, including *N*-chloromethyl hordenine **5**, *N*-acetyl hordenine **6**, and *N*-acetyl-*N*-chloromethyl-*N*-methyl tyramine **7**. This study highlights chlorine-containing alkaloid scaffolds, particularly hordenine derivatives, as promising candidates for enhanced neuroprotective properties, underscoring the critical role of a chlorine moiety in improving their efficacy. Additionally, the significant anti-AChE potential of secondary metabolites naringenin, isokaempferide, and vomifoliol-9-*O*-β-D-glucopyranoside was demonstrated. The results of *in silico* studies were greatly aligned with the *in vitro* results, revealing that compounds **4** and **5** are promising AChE inhibitors, while compounds **3**, **4**, and **7** are leading candidates against β-secretase. Finally, our study identifies naringenin **1**, isokaempferide **3**, *N*-chloromethyl hordenine **5** and *N*-acetyl-*N*-chloromethyl-*N*-methyl tyramine **7**, and vomifoliol-9-*O*-β-D-glucopyranoside **4**, as effective lead compounds for the management of multiple disorders. These findings need further *in vivo* studies to validate these preliminary results.

Author contributions

Conceptualization: A. A. H., A. I. M. and A. A. E. Methodology, visualization and experimental design: A. A. H., A. O., A. M. S., M. M. H., A. I. M., and A. A. E. Analysis of spectral data: A. A. H., A. O, M. M. H., A. I. M. and A. A. E. Docking and MD studies: A. M. S. Biological investigation: A. A. H., A. O., and A. A. E. Writing – original manuscript: A. A. H., A. O., and A. M. S. Revision and editing: A. A. H., A. O., M. M. H., A. I. M., and A. A. E. Supervision: A. I. M., and A. A. E. All the authors approved the final version of the manuscript.

Conflicts of interest

There are no conflicts to declare.

Data availability

All data obtained during this study are included in this published article and supplementary information (SI). Supplementary information is available. See DOI: https://doi.org/10.1039/d5ra07497e.

References

1 B. A. English and A. A. Webster, Acetylcholinesterase and its Inhibitors, *Primer on the Autonomic Nervous System*, 2012, pp. 631–633.

2 M. B. Colovic, D. Z. Krstic, T. D. Lazarevic-Pasti, A. M. Bondzic and V. M. Vasic, Acetylcholinesterase Inhibitors: Pharmacology and Toxicology, *Curr. Neuropharmacol.*, 2013, **1**(3), 315–335, DOI: 10.2174/1570159x11311030006.

3 M. M. da Rosa, J. V. d. O. Alves, I. F. d. S. Aguiar, F. G. d. S. Oliveira, M. V. da Silva and M. T. C. dos Santos, The Promising Role of Natural Products in Alzheimer's Disease, *Brain Disord.*, 2022, **7**, 100049, DOI: 10.1016/j.dscb.2022.100049.

4 J. A. Fissel and M. H. Farah, The Influence of BACE1 on Macrophage Recruitment and Activity in The Injured Peripheral Nerve, *J. Neuroinflammation*, 2021, **18**(1), 71, DOI: 10.1186/s12974-021-02121-2.

5 M. Gottardi Zamperla, Characterization of BACE1/BACE1-AS/β-Amyloid Axis in Cardiovascular Risk Conditions: Exploring its Pathophysiological miRNAs Connection, PhD thesis, Universitá degli studi di Pavia, 2025.

6 D. Kumar, A. Ganeshpurkar, D. Kumar, G. Modi, S. K. Gupta and S. K. Singh, Secretase Inhibitors for The Treatment of Alzheimer's Disease: Long Road Ahead, *Eur. J. Med. Chem.*, 2018, **148**, 436–452, DOI: 10.1016/j.ejmech.2018.02.035.

7 R. Chandra, P. Bhandari, S. C. Sharma, I. Emmanuel and A. Alam, Health Benefits of Cactus, *Ann. Phytomed.*, 2019, **8**, 179–185, DOI: 10.21276/ap.2019.8.2.23.

8 S. S. Monteiro, R. L. Almeida, N. C. Santos, E. M. Pereira, A. P. Silva, H. M. L. Oliveira and M. A. d. B. Pasquali, New Functional Foods with Cactus Components: Sustainable Perspectives and Future Trends, *Foods*, 2023, **12**(13), 2494, DOI: 10.3390/foods12132494.

9 A. El-Ghani, The Floristic Composition of Some Historical Botanical Gardens in The Metropolitan of Cairo, Egypt, *Afr. J. Agric. Res.*, 2007, **2**(11), 610–648.

10 A. Orozco-Barocio, M. A. Sánchez-Sánchez, A. E. Rojas-Mayorquín, M. Godínez-Rubí, M. P. Reyes-Mata and D. Ortuño-Sahagún, Phytochemicals from Cactaceae Family for Cancer Prevention and Therapy, *Front. Pharmacol.*, 2024, **15**, 1421136, DOI: 10.3389/fphar.2024.1421136.

11 A. Othman, A. M. Sayed, Y. Amen and K. Shimizu, Possible Neuroprotective Effects of Amide Alkaloids from *Bassia indica* and *Agathophora alopecuroides*: *In vitro* and *In silico* Investigations, *RSC Adv.*, 2022, **12**, 18746–18758, DOI: 10.1039/D2RA02275C.

12 N. M. O'Boyle, M. Banck, C. A. James, C. Morley, T. Vandermeersch and G. R. Hutchison, Open Babel: An Open Chemical Toolbox, *J. Cheminf.*, 2011, **3**, 33.

13 G. M. Morris, R. Huey, W. Lindstrom, M. F. Sanner, R. K. Belew, D. S. Goodsell and A. J. Olson, AutoDock4 and AutoDockTools4: Automated Docking with Selective Receptor Fexibility, *J. Comput. Chem.*, 2009, **30**, 2785–2791.

14 Y. Koriyama, A. Hori, H. Ito, S. Yonezawa, Y. Baba, N. Tanimoto, T. Ueno, S. Yamamoto, T. Yamamoto, N. Asada, K. Morimoto, S. Einaru, K. Sakai, T. Kanazu, A. Matsuda, Y. Yamaguchi, T. Oguma, M. Timmers, L. Tritsmans, K. I. Kusakabe, A. Kato and G. Sakaguchi, Discovery of Atabecestat (JNJ-54861911): A Thiazine-Based β-amyloid Precursor Protein Cleaving Enzyme 1 Inhibitor Advanced to the Phase 2b/3 Early Clinical Trial, *J. Med. Chem.*, 2021, **64**, 1873–1888, DOI: 10.1021/acs.jmedchem.

15 J. Cheung, M. J. Rudolph, F. Burshteyn, M. S. Cassidy, E. N. Gary, J. Love, M. C. Franklin and J. J. Height, Structures of Human Acetylcholinesterase in Complex with Pharmacologically Important Ligands, *J. Med. Chem.*, 2012, **55**, 10282–10286, DOI: 10.1021/jm3008.

16 P. Eastman, M. S. Friedrichs, J. D. Chodera, R. J. Radmer, C. M. Bruns, J. P. Ku, K. A. Beauchamp, T. J. Lane, L.-P. Wang and D. Shukla, OpenMM 4: A Reusable, Extensible, Hardware Independent Library for High Performance Molecular Simulation, *J. Chem. Theory Comput.*, 2013, **9**, 461–469.

17 S. Dallakyan and A. J. Olson, *Chemical Biology*, ed. J. E. Hempel, C. H. Williams and C. C. Hong, Springer, New York, NY, USA, 2015.

18 D. Seeliger and B. L. de Groot, Ligand Docking and Binding Site Analysis with PyMOL and Autodock/Vina, *J. Comput.-Aided Mol. Des.*, 2010, **24**, 417–422.

19 J. C. Phillips, R. Braun, W. Wang, J. Gumbart, E. Tajkhorshid, E. Villa, C. Chipot, R. D. Skeel, L. Kale and K. Schulten, Scalable Molecular Dynamics with NAMD, *J. Comput. Chem.*, 2005, **26**, 1781–1802.

20 J. V. Ribeiro, R. C. Bernardi, T. Rudack, K. Schulten and E. Tajkhorshid, QwikMD-Gateway for Easy Simulation with VMD and NAMD, *Biophys. J.*, 2018, **114**, 673a–674a.

21 W. Humphrey, A. Dalke and K. Schulten, VMD: Visual Molecular Dynamics, *J. Mol. Graph.*, 1996, **14**, 33–38.

22 B. R. Miller III, T. D. McGee Jr, J. M. Swails, N. Homeyer, H. Gohlke and A. E. Roitberg, MMPBSA. py: An Efficient Program for End-state Free Energy Calculations, *J. Chem. Theory Comput.*, 2012, **8**, 3314–3321.

23 F. Maltese, C. Erkelens, F. van der Kooy, Y. H. Choi and R. Verpoorte, Identification of Natural Epimeric Flavanone Glycosides by NMR Spectroscopy, *Food Chem.*, 2009, **116**, 575–579, DOI: 10.1016/j.foodchem.2009.03.023.

24 E. A. Ragab, M. Hosny, H. A. Kadry and H. A. Ammar, Flavanone glycosides from *Gleditsia caspia*, *Indian J. Nat. Prod.*, 2010, **3**, 35–46.

25 S. Din, S. Hamid, A. Yaseen, A. M. Yatoo, S. Ali, K. Shamim, W. A. Mahdi, S. Alshehri, M. U. Rehman and W. A. Shah, Isolation and characterization of Flavonoid Naringenin and Evaluation of Cytotoxic and Biological Efficacy of Water Lilly (*Nymphaea mexicana* Zucc.), *Plants*, 2022, **11**, 3588, DOI: 10.3390/plants11243588.

26 P. K. Agrawal, *Carbon-13 NMR of Flavonoids*, 1989, vol. 39.

27 S. S. Hong, Y. H. Choi, H. J. Suh, M. J. Kang, J. H. Shin, O. O. Kwon and J. S. Oh, Flavonoid Constituents of *Acacia catechu*, *J. Appl. Biol. Chem.*, 2015, **58**, 189–194, DOI: 10.3839/jabc.2015.030.

28 J. W. Kim, T. B. Kim, H. Yang and S. H. Sung, Phenolic Compounds Isolated from *Opuntia ficus-indica* Fruits, *Nat. Prod. Sci.*, 2016, **22**, 117–121, DOI: 10.20307/nps.2016.22.2.117.

29 K. R. Markham, B. Ternai, R. Stanley, H. Geiger and T. J. Mabry, Carbon-13 NMR Studies of Flavonoids-III. Naturally Occurring Flavonoid Glycosides and Their Acylated Derivatives, *Tetrahedron*, 1978, **34**, 1389–1397, DOI: 10.1016/0040-4020(78)88336-7.

30 H. Kai, M. Baba and T. Okuyama, Two New Megastigmanes from The Leaves of *Cucumis sativus*, *Chem. Pharm. Bull.*, 2007, **55**, 133–136, DOI: 10.1248/cpb.55.133.

31 R. M. Samra, A. Othman, M. Elsbaey, Y. Amen and K. Shimizu, Comprehensive Review on Megastigmane Glycosides: Sources, Bioactivities, and ^{13}C NMR Spectroscopic Data, *Phytochem. Lett.*, 2024, **60**, 19–89, DOI: 10.1016/j.phytol.2024.01.008.

32 A. Othman, Phytoconstituents and Biological Evaluation of *Justicia spicigera* Cultivated in Egypt, *Al-Azhar J. Pharm. Sci.*, 2017, **56**, 10–19, DOI: 10.21608/ajps.2017.28456.

33 S. Ouissem Bensaid, M. Carbone, L. Palomba, S. Bicha, A. Bentamene, A. Carannante, M. Gavagnin and M. Letizia Ciavatta, First Occurrence of Megastigmane Glucosides in a Plant of *Retama* genus, *Chem. Biodivers.*, 2022, **19**, e202200675, DOI: 10.1002/cbdv.202200675.

34 G. Huang, P. Jiang and X. F. Li, Mass Spectrometry Identification of *N*-Chlorinated Dipeptides in Drinking Water, *Anal. Chem.*, 2017, **89**, 4204–4209, DOI: 10.1021/acs.analchem.7b00228.

35 R. Wang, S. Wu, J. Xu, F. Xu and D. Wu, A Novel Phenanthrene and An Undescribed Alkaloid from the Roots of *Stephania tetrandra*, *Rec. Nat. Prod.*, 2023, **17**, 622–627, DOI: 10.25135/rnp.381.2212.2663.

36 M. Shaiq Ali, M. Saleem, W. Ahmad, M. Parvez and R. Yamdagni, A Chlorinated Monoterpene ketone, acylated β-sitosterol Glycosides and a Flavanone Glycoside from *Mentha longifolia* (Lamiaceae), *Phytochemistry*, 2002, **59**, 889–895, DOI: 10.1016/S0031-9422(01)00490-3.

37 M. Shabana, M. Gonaid, M. M. Salama and E. Abdel-Sattar, Phenylalkylamine Alkaloids from *Stapelia hirsuta* L, *Nat. Prod. Res.*, 2006, **20**, 710–714, DOI: 10.1080/14786410500137718.

38 P. R. Srinivasan and R. L. Lichter, ^{13}C NMR Spectral Studies of Arecoline, Hordenine, Strychnine and Brucine, *Org. Magn. Reson.*, 1976, **8**, 198–201, DOI: 10.1002/mrc.1270080408.

39 A. Imramovsky, S. Stepankova, J. Vanco, K. Pauk, J. Monreal-Ferriz, J. Vinsova and J. Jampilek, Acetylcholinesterase-inhibiting activity of salicylanilide *N*-alkylcarbamates and their molecular docking, *Molecules*, 2012, 10142–10158, DOI: 10.3390/molecules170910142.

40 T. H. Tran, T. T. H. Vo, T. Q. N. Vo, T. C. N. Cao and T. S. Tran, Synthesis and Evaluation of the Acetylcholinesterase Inhibitory Activities of Some Flavonoids Derived from Naringenin, *Sci. World J.*, 2021, 4817900, DOI: 10.1155/2021/4817900.

41 B. K. Cassels, Alkaloids of the Cactaceae ? The Classics, *Nat. Prod. Commun.*, 2019, **14**, 85–90, DOI: 10.1177/1934578X1901400123.